Mater. Res. Soc. Symp. Proc. Vol. 1321 © 2011 Materials Research Society
DOI: 10.1557/opl.2011.813

Mixed phase silicon oxide layers for thin-film silicon solar cells

Peter Cuony[1], Duncan T.L. Alexander[2], Linus Löfgren[1], Michael Krumrey[3], Michael Marending[1], Mathieu Despeisse[1], Christophe Ballif[1]

[1] Ecole Polytechnique Fédérale de Lausanne (EPFL), Institute of Microengineering (IMT), Photovoltaics and Thin Film Electronics Laboratory (PV-Lab), Rue Breguet 2, 2000 Neuchâtel, Switzerland

[2] Ecole Polytechnique Fédérale de Lausanne (EPFL), Interdisciplinary Centre for Electron Microscopy (CIME), 1015 Lausanne, Switzerland

[3] Physikalisch-Technische Bundesanstalt (PTB), Abbestr. 2-12, 10587 Berlin, Germany

ABSTRACT

Lower absorption, lower refractive index and tunable resistance are three advantages of doped silicon oxide containing nanocrystalline silicon grains (nc-SiO_x) compared to doped microcrystalline silicon, for the use as p- and n-type layers in thin-film silicon solar cells. In this study we show how optical, electrical and microstructural properties of nc-SiO_x layers depend on precursor gas ratios and we propose a growth model to explain the phase separation in such films into Si-rich and O-rich regions as visualized by energy-filtered transmission electron microscopy.

INTRODUCTION

The tandem configuration with a hydrogenated amorphous silicon (a-Si) top cell and a hydrogenated microcrystalline silicon (µc-Si) bottom cell, also called the Micromorph configuration is a promising candidate for future large scale deployment of photovoltaics for electricity generation due to abundant source materials and scalable and low-cost deposition processes. Hydrogenated silicon oxide containing nanocrystalline silicon grains (nc-SiO_x) has attracted much interest in the last years because of different applications in thin-film silicon solar cells: First, p-type nc-SiO_x is an excellent window and anti-reflection layer, due to lower absorption coefficient and lower refractive index when compared to p-type µc-Si layers [1]. Second, n-type nc-SiO_x can be used as intermediate reflecting layer, when inserted between two sub-cells of a tandem configuration, allowing for advanced light-trapping schemes [2-5]. Third, tunable resistance of p- and n-type nc-SiO_x can help to reduce the impacts of shunts on the electrical cell parameters [1, 6].

EXPERIMENTAL DETAILS

The nc-SiO_x layers are deposited at 200 °C from a gas mixture of SiH_4, H_2, and CO_2 by plasma enhanced chemical vapor deposition, and p- and n-type doping is achieved by adding $B(CH_3)_3$ and PH_3, respectively. Fourier Transform Infrared (FTIR) absorption measurements are performed with a Nicolet 8700 system from Thermo on samples deposited on silicon wafers and absorption spectra are normalized with the layer thickness. Rutherford backscattering (RBS) and hydrogen forward scattering (HFS) measurements to determine Si, O, and H contents are carried

out by the Evans Analytical Group. The density is deduced from X-ray reflectometry performed with synchrotron radiation at the PTB four-crystal monochromator beamline at BESSY II [7]. The absorption coefficient (α) and refractive index (n) are determined from fitting spectroscopic ellipsometry measurements to a Tauc-Lorentz dispersion model including a surface roughness layer. Two aluminum contacts are evaporated onto the samples, in order to measure the electrical in-plane dark conductivity (σ) after 90 minutes annealing at 180 °C in vacuum. The crystalline fraction of the Si-rich phase (hence not taking into account the O-rich phase) is evaluated by Raman spectroscopy [8].

RESULTS AND DISCUSSION

Figure 1a shows infrared absorption peak of Si-O-Si stretching mode at 1050 cm^{-1} [9, 10], which is increasing with increasing CO_2/SiH_4 precursor gas ratio due to increased oxygen content in the nc-SiO_x films. From this absorption peak one can estimate the oxygen content and we found the best correlation to RBS measurements when using the proportionality constant $A_{SiO} = 1.48 \cdot 10^{19}$ cm^{-2} proposed by He et al. [11]. Figure 1b demonstrates that oxygen incorporation is also enhanced by increasing H_2 source gas dilution. To explain this effect, Iftiquar et al. [10] argue that in the plasma, atomic hydrogen inhibits the backward reaction of $CO + O \rightarrow CO_2$ by forming OH. Because highly reactive and electronegative O hardly leaves the plasma it is speculated that oxygen mainly reaches the growing nc-SiO_x film in the form of OH. In this context it is interesting to note that the hydrogen content does not correlate with H_2 dilution in the plasma but shows a correlation to silicon content of the nc-SiO_x films which can be explained by free energy models predicting that H in SiO_x films will be only bound to Si with an absence of O-H bounds [12].

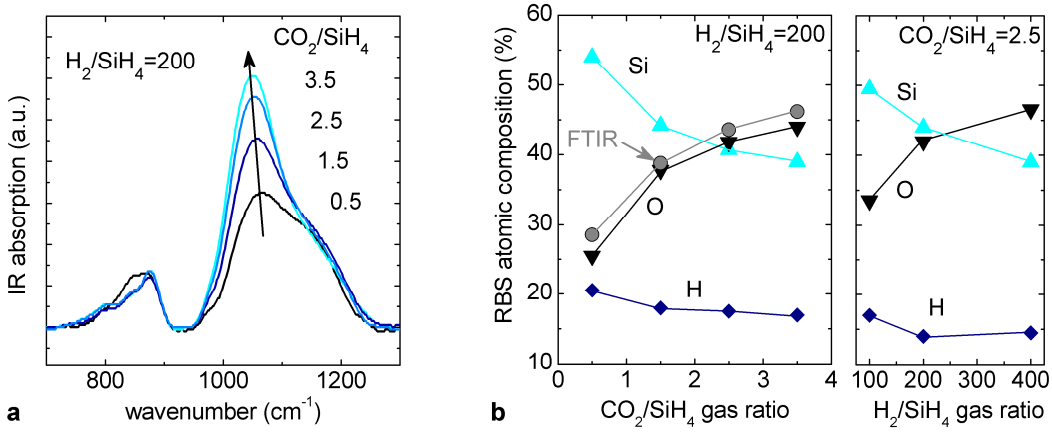

Figure 1. a) Infrared absorption peak of Si-O-Si stretching mode at 1050 cm^{-1} of 100 nm thick nc-SiO_x layers. **b)** Silicon, oxygen and hydrogen content measured by RBS and HFS for different source gas ratios and oxygen content calculated from FTIR measurements for comparison.

Figure 2a shows dark conductivity (σ), silicon crystalline fraction (*Si Rc*) and absorption coefficient (α) of p- and n-type nc-SiO_x layers as a function of CO_2/SiH_4 gas flow ratio. In this experiment, the H_2-dilution is set to 200 for p-type layers and 100 for the n-type layers, because in the p-i-n configuration of µc-Si cells it is common to use higher H_2 dilution for the p-layer because it grows on a ZnO substrate, with longer incubation phase compared to n-layer which

grows directly on a µc-Si layer, favoring the growth of microcrystalline material. For both p- and n-type layers, the dark in-plane conductivity is around 10 $S \cdot cm^{-1}$ for an oxygen free sample, and decreases rapidly with higher CO_2/SiH_4 gas ratio, due to an increasing amount of oxygen incorporated in the nc-SiO_x film. Furthermore, increasing CO_2/SiH_4 gas ratio reduces the Raman crystalline fraction of the Si-rich phase in the nc-SiO_x layers, and decreases the optical absorption coefficient α. Figure 2b shows the results obtained for different doping concentrations, ranging from 0 ‰ to 50 ‰, with a constant CO_2/SiH_4 gas ratio of 0.5. p-type doping with trimethylboron (TMB) rapidly reduces the crystalline fraction of the silicon phase, and a maximum dark conductivity is obtained at TMB/SiH_4 = 8 ‰. This is different for n-type doping with PH_3, where dark conductivity is continuously increasing with increasing doping gas concentration as phosporous does not reduce the crystalline fraction of the silicon phase. This amorphizing effect of TMB limits the oxygen content in nc-SiO_x films to x~0.5 before the films become too resistive to be used in thin-film silicon solar cells. For n-type nc-SiO_x layers, where high phosphorous doping concentrations can partially make up for lower conductivity due to oxygen incorporation, we achieved nc-SiO_x films with x~1 which have still a transverse conductivity high enough for the use in thin-film silicon solar cells.

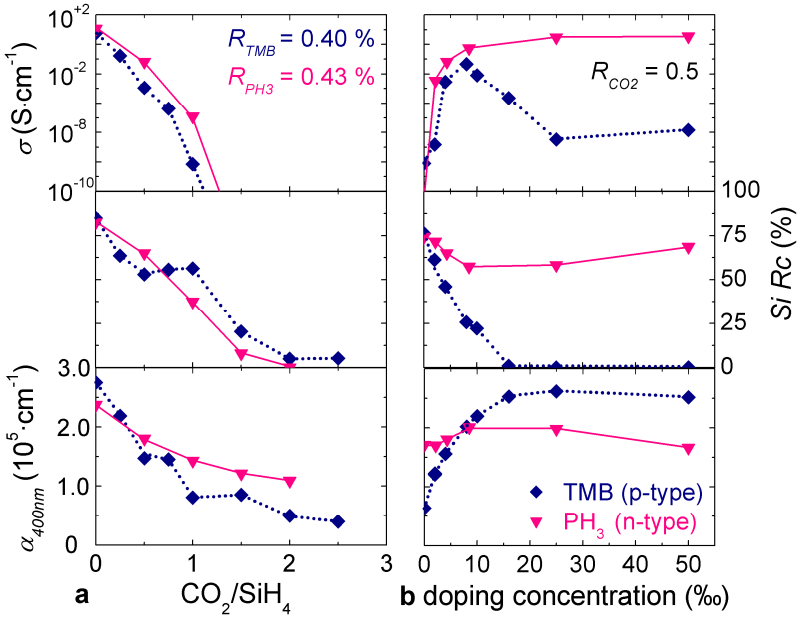

Figure 2. Evolution of dark conductivity (σ), silicon Raman crystalline fraction (*Si Rc*) and absorption coefficient (α) of p- and n-type nc-SiO_x layers deposited with different CO_2/SiH_4 gas ratios (**a**) and doping concentrations (**b**).

Figure 3a shows the decrease in dark conductivity due to air exposure of two nc-SiO_x layers with different oxygen contents. The initial conductivity can be recovered by annealing the samples during 90 minutes at 180° in vacuum. Water vapor penetrating into nano-pores of nc-SiO_x films is believed to be the major reason for this reversible in-plane conductivity degradation. Figure 3b shows X-ray reflectometry measurements revealing a lower critical angle for nc-SiO_x than for a-Si suggesting a lower density [13] and strengthening the hypothesis of nano-scale porosity in nc-SiO_x layers.

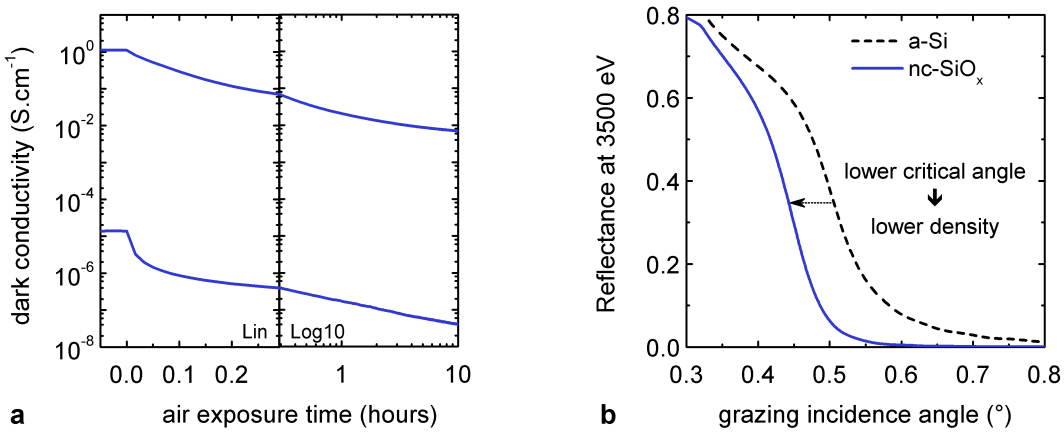

Figure 3. a) Decreasing dark conductivity due to air exposure of two different 100 nm thick nc-SiO_x layers. **b)** X-ray reflectometry measurements at 3500 eV (far away from the Si absorption edge) indicating significantly less dense material for nc-SiO_x when compared to a-Si material.

Figure 4 shows the nanostructure of the nc-SiO_x layer as visualized in plan-view by energy-filtered transmission electron microscopy (Si-rich phase = white; O-rich phase = dark). The image is obtained using electrons from a 4 eV window over the plasmon peak of silicon at ~17.5 eV, after removal of the background contribution from the plasmon peak of SiO_2[14]. While layers produced with low H_2 dilution appear as homogenous SiO_x mixture (Figure 4a), this technique reveals a pronounced phase separation on the nanometer scale into Si-rich regions surrounded by an O-rich material for samples that have been produced with a high H_2 dilution (Figure 4b-c). The difference in silicon particle sizes between sample b and c is due to the different silicon content of the nc-SiO_x films. It is interesting to note that the homogenous $SiO_{x\sim1.4}$ (sample a) and the phase-separated nc-$SiO_{x\sim1}$ (sample b), both have a refractive index of ~ 1.8 but different SiO_x stoichiometry, which could be due to the increased nano-porosity in nc-SiO_x samples with phase separation.

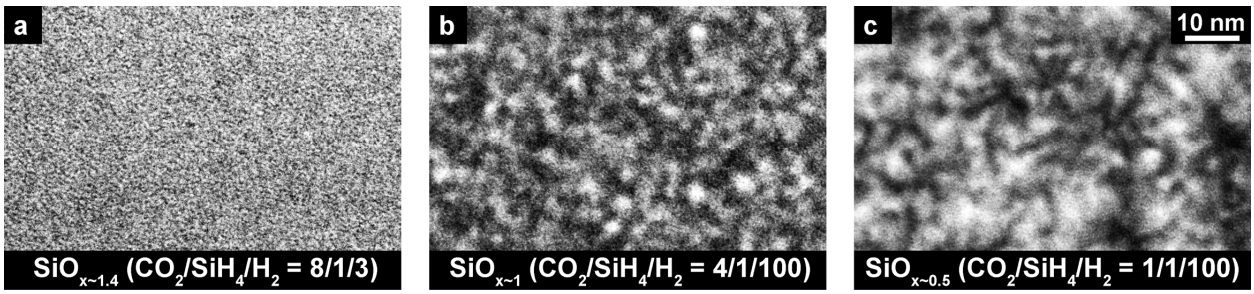

Figure 4. Plan-view phase separation visualized by energy-filtered transmission electron microscopy (Si phase = white) in 50-70 nm thick nc-SiO_x layers produced with different $CO_2/SiH_4/H_2$ gas ratios.

Mixed-phase nc-SiO_x films have been studied previously, but the energetically favorable phase separation is usually obtained after high-temperature annealing of initially homogenous SiO_x films [14-16]. In our case, we show that the phase separation is also possible at low substrate temperatures of 200 °C, if produced with highly H_2 diluted plasmas. This growth mechanism can be explained with the surface diffusion model [17], as developed for mixed-

phase a-Si/µc-Si films. For low H_2 dilution all the Si and O atoms arriving from the plasma stick to the surface leading to a homogenous SiO_x film (Figure 5a), whereas high H_2 dilution enables phase-separation by increasing adatom mobility via surface heating and passivation of surface dangling bonds (Figure 5b).

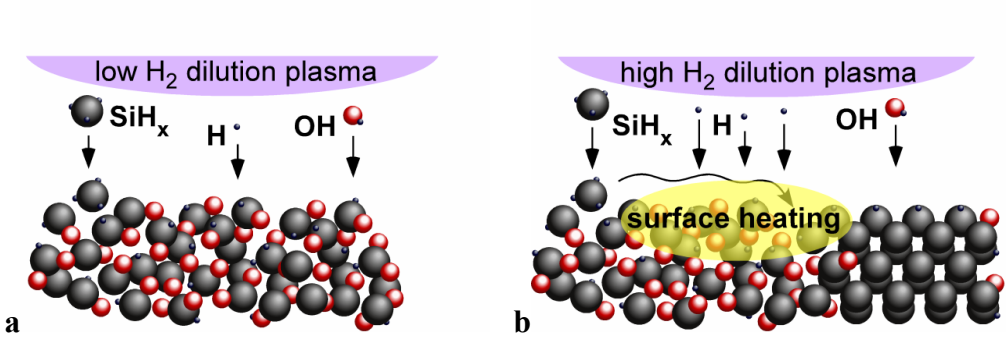

Figure 5. Surface diffusion model [17] with low adatom mobility in the case of low H_2 dilution leading to homogenous SiO_x material (**a**) and high adatom mobility due to surface heating and H-bonding of surface dangling bonds in the case of high H_2 dilution leading to Si/SiO_2 mixed-phase structure (**b**).

CONCLUSIONS

In this contribution we have related precursor gas ratios to optical, electrical and microstructural characteristics of nc-SiO_x films. We evidenced a possible nano-porosity in these films which makes them sensitive to air exposure. With energy-filtered transmission electron microscopy we demonstrated a phase separation within nc-SiO_x films into Si-rich and O-rich regions. H_2 source gas dilution has been identified as a key parameter for the phase separation, whereas the size of the Si-rich regions depends mostly on the silicon content in nc-SiO_x films. To explain the phase-separation we used a modified surface diffusion model, originally developed for mixed-phase a-Si/µc-Si materials.

ACKNOWLEDGMENTS

The authors acknowledge support by the Swiss Federal Energy Office (Grant No. 101191).

REFERENCES

1. P. Cuony, M. Marending, D. T. L. Alexander, M. Boccard, G. Bugnon, M. Despeisse and C. Ballif, Appl Phys Lett **97** (21), 213502 (2010).
2. P. Buehlmann, J. Bailat, D. Domine, A. Billet, F. Meillaud, A. Feltrin and C. Ballif, Appl Phys Lett **91**, 143505 (2007).
3. T. Grundler, A. Lambertz and F. Finger, physica status solidi (c) **7** (3-4), 1085–1088 (2010).
4. D. Dominé, P. Buehlmann, J. Bailat, A. Billet, A. Feltrin and C. Ballif, Phys Status Solidi-R **2** (4), 163–165 (2008).
5. P. Buehlmann, J. Bailat, A. Feltrin and C. Ballif, Photovoltaic Materials and Manufacturing Issues **1123** (2009).

6. M. Despeisse, G. Bugnon, A. Feltrin, M. Stueckelberger, P. Cuony, F. Meillaud, A. Billet and C. Ballif, Appl Phys Lett **96**, 073507 (2010).
7. M. Krumrey, M. Hoffmann, G. Ulm, K. Hasche and P. Thomsen-Schmidt, Thin Solid Films **459** (1-2), 241-244 (2004).
8. C. Droz, E. Vallat-Sauvain, J. Bailat, L. Feitknecht, J. Meier and A. Shah, Sol Energ Mat Sol C **81** (1), 61–71 (2004).
9. G. Lucovsky, J. Yang, S. S. Chao, J. E. Tyler and W. Czubatyj, Phys Rev B **28** (6), 3225-3233 (1983).
10. S. M. Iftiquar, J Phys D Appl Phys **31** (14), 1630–1641 (1998).
11. L. N. He, D. M. Wang and S. Hasegawa, J Non-Cryst Solids **261** (1-3), 67-71 (2000).
12. F. W. Smith and Z. Yin, J Non-Cryst Solids **137-138** (Part 2), 871-874 (1991).
13. L. G. Parratt, Phys Rev **99** (5), 1635-1635 (1955).
14. S. Schamm, C. Bonafos, H. Coffin, N. Cherkashin, M. Carrada, G. Ben Assayag, A. Claverie, M. Tence and C. Colliex, Ultramicroscopy **108** (4), 346–357 (2008).
15. G. Nicotra, S. Lombardo, C. Spinella, G. Ammendola, C. Gerardi and C. Demuro, Appl Surf Sci **205** (1–4), 304–308 (2003).
16. F. Iacona, C. Bongiorno, C. Spinella, S. Boninelli and F. Priolo, J Appl Phys **95** (7), 3723–3732 (2004).
17. A. Matsuda, Thin Solid Films **337** (1–2), 1–6 (1999).